



Calibrating effective focal length for central catadioptric cameras using one space line

Fuqing Duan^{a,*}, Fuchao Wu^b, Mingquan Zhou^a, Xiaoming Deng^{b,c}, Yun Tian^a

^a College of Information Science and Technology, Beijing Normal University, Beijing 100875, PR China

^b National Laboratory of Pattern Recognition, Institute of Automation, Chinese Academy of Sciences, Beijing 100080, PR China

^c Laboratory of Human-Computer Interaction and Intelligent Information Processing, Institute of Software, Chinese Academy of Sciences, Beijing 100190, PR China

ARTICLE INFO

Article history:

Received 18 September 2010

Available online 27 May 2011

Communicated by Y. Liu

Keywords:

Camera calibration

Central catadioptric camera

Focal length estimation

ABSTRACT

In camera calibration, focal length is the most important parameter to be estimated, while other parameters can be obtained by prior information about scene or system configuration. In this paper, we present a polynomial constraint on the effective focal length with the condition that all the other parameters are known. The polynomial degree is 4 for paracatadioptric cameras and 16 for other catadioptric cameras. However, if the skew is 0 or the ratio between the skew and effective focal length is known, the constraint becomes a linear one or a polynomial one with degree 4 on the effective focal length square for paracatadioptric cameras and other catadioptric cameras, respectively. Based on this constraint, we propose a simple method for estimation of the effective focal length of central catadioptric cameras. Unlike many approaches using lines in literature, the proposed method needs no conic fitting of line images, which is error-prone and highly affects the calibration accuracy. It is easy to implement, and only a single view of one space line is enough with no other space information needed. Experiments on simulated and real data show this method is robust and effective.

© 2011 Elsevier B.V. All rights reserved.

1. Introduction

In many computer vision applications, such as robot navigation, surveillance, teleconferencing, and virtual reality etc, it would be convenient if the imaging system could have a large field of view (FOV). However, a conventional camera has a very limited FOV. One effective way to enhance the FOV is to combine mirrors with a conventional camera, which is called a catadioptric imaging system (Yagi and Yachida, 2004; Swaminathan et al., 2006; Baker and Nayer, 1999). In catadioptric systems, a single effective viewpoint is highly desirable due to its superior and useful geometric properties (Baker and Nayer, 1999; Geyer and Daniilidis, 2001). A catadioptric system with a unique viewpoint is called a central catadioptric system. The complete class of central catadioptric systems is presented by Baker and Nayer (1999). They introduce that a central catadioptric system can be built by setting a parabolic mirror in front of an orthographic camera, or a hyperbolic, elliptical, planar mirror in front of a perspective camera, where the single viewpoint constraint can be fulfilled via a careful alignment that the camera is located at the mirror focus. Now the calibration of central catadioptric cameras has been an active research field (Barreto and Araujo, 2005; Geyer and Daniilidis, 1999, 2002; Ying and

Hu, 2004; Wu and Hu, 2005; Wu et al., 2008; Deng et al., 2007; Ying and Zha, 2008).

Some methods use images of known scene points to calibrate central catadioptric cameras. For example, Wu and Hu (2005) calibrate the camera principal point accurately from 1D space points, Scaramuzza et al. (2006) and Kannala et al., 2008 use a 2D calibration pattern, Sturm and Ramalingam (2004) use 2D or 3D space points to calibrate a generic kind of omnidirectional cameras. Another kind of methods (Ramalingam et al., 2005; Kang, 2000) is self-calibration using point correspondences across multiple views without requiring any scene information. For example, Ramalingam et al. (2005) calibrate generic central cameras by specific camera motions.

Lines are common geometric entities in the man-made scenes, and are widely used in camera calibration (Barreto and Araujo, 2005; Geyer and Daniilidis, 1999, 2002; Ying and Hu, 2004; Wu and Hu, 2005; Wu et al., 2008; Deng et al., 2007; Duan et al., 2008). Geyer and Daniilidis use a single view of two sets of parallel lines (Geyer and Daniilidis, 1999) or a single view of three scene lines (Geyer and Daniilidis, 2002) to calibrate a parabolic catadioptric camera. They also propose a unified sphere model (Geyer and Daniilidis, 2001) for describing the imaging process of central catadioptric cameras, under which some algorithms (Ying and Hu, 2004; Wu and Hu, 2005; Wu et al., 2008; Deng et al., 2007; Ying and Zha, 2008) are proposed for calibrating central catadioptric cameras. Ying and Hu (2004) apply some geometric invariants of

* Corresponding author. Tel.: +86 10 58800442; fax: +86 10 58808306.

E-mail address: fqduan@bnu.edu.cn (F. Duan).

lines or spheres to calibrate central catadioptric cameras. Barreto and Araujo (2005) study the projective invariant properties of catadioptric images of space lines and show that any central catadioptric camera can be fully calibrated from an image of three or more space lines. Wu et al. (2008) present a group of linear constraints on the catadioptric parameters from the catadioptric projections of spatial lines. Ying and Zha (2008) present some identical projective geometric properties of central catadioptric images of lines and spheres, and apply these properties to calibration. Since a space line is projected onto a conic in a central catadioptric image, nearly all these approaches need conic fitting of line images, and the calibration accuracy highly depends on the accuracy of the conic fitting. In general, only a small segment of the conic is visible in the catadioptric image due to partial occlusion. This makes the conic estimation error-prone. Although Barreto and Araujo (2006) present an effective method for conic fitting of line images in paracatadioptric systems, it is still unsolved in other systems such as hypercatadioptric system. Wu et al. (2006) present a calibration method with the principal point known, which needs no conic fitting of line images, but it is only for paracatadioptric cameras.

In camera calibration, focal length is the most important parameter to be estimated, while other parameters can be obtained by prior information about scene or system configuration. For example, Sturm et al. (2005) calibrate the focal length of a traditional camera from two views while keeping the focal length fixed during the motion of the camera, in which they assume all other camera parameters are known. The contribution of this paper is as follows: Firstly, we obtain a polynomial constraint on the effective focal length from a property that the projections of any three collinear points on the viewing sphere should be coplanar with the view sphere center. Secondly, based on this constraint, this paper proposes a robust algorithm for calibration of the effective focal length of central catadioptric cameras. The algorithm does not need conic fitting of line images, is easy to implement, and only a single view of one space line is enough with no other space information needed.

Section 2 reviews the unified imaging model given by Geyer and Daniilidis. Section 3 derives the constraints on camera parameters. Section 4 describes the proposed algorithm. Experimental results are reported in Section 5, and followed are some conclusions in Section 6.

2. A generalized imaging model for central catadioptric camera

The imaging model proposed by Geyer and Daniilidis (2001) is widely used in central catadioptric camera calibration due to its simplicity and generality. They prove that the central catadioptric imaging process is equivalent to the following two-step mapping by a view sphere (see Fig. 1.):

Firstly, under the viewing sphere coordinate system $\mathbf{O}-xyz$ with \mathbf{O} being the unit sphere center, a 3D point $\mathbf{X} = [x, y, z]^T$ is projected to a point \mathbf{X}^s on the unit sphere through the viewpoint \mathbf{O} by $\mathbf{X}^s = [x/r, y/r, z/r]^T$, $r = \|\mathbf{X}\|$, $\|\cdot\|$ denotes the norm of vector in it; Secondly, the point \mathbf{X}^s on the viewing sphere is perspectively projected to a point \mathbf{m} on the catadioptric image plane Π by a virtual pinhole camera through the perspective center \mathbf{O}^c . In this camera system, there is only a translation between the pinhole coordinate system $\mathbf{O}^c-x^c y^c z^c$ and the viewing sphere coordinate system $\mathbf{O}-xyz$, and the optical axes of the virtual pinhole camera is the line going through the viewpoints \mathbf{O} and \mathbf{O}^c . Hence, the image plane is perpendicular to the line $\mathbf{O}^c\mathbf{O}$, and its principal point is the intersection, $\mathbf{p} = [u_0, v_0, 1]^T$, of the line $\mathbf{O}^c\mathbf{O}$ with the image plane Π . The distance ξ from point \mathbf{O} to \mathbf{O}^c is called the mirror parameter, which determines the mirror type used in a central catadioptric camera. The mirror is a paraboloid if $\xi = 1$, an ellipsoid or a hyperboloid if

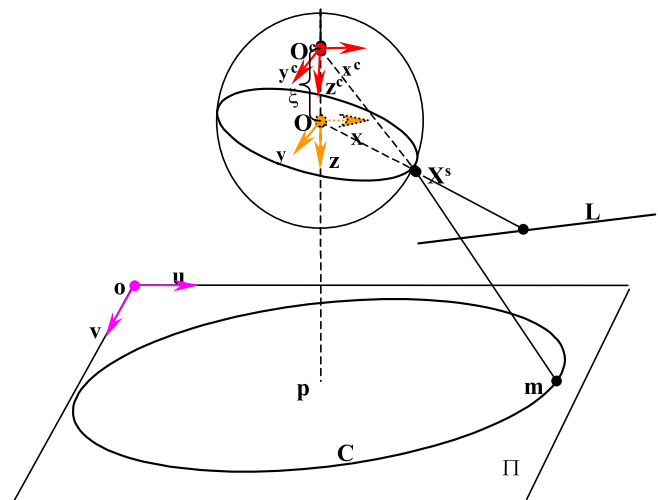


Fig. 1. The generalized imaging model for central catadioptric cameras.

$0 < \xi < 1$, and a plane if $\xi = 0$. The details can be found in (Geyer and Daniilidis, 2001). In this paper, we assume $0 < \xi \leq 1$, i.e. do not consider the case of plane mirror.

Let the intrinsic matrix of the virtual pinhole camera be

$$\mathbf{K} = \begin{bmatrix} rf & s & u_0 \\ 0 & f & v_0 \\ 0 & 0 & 1 \end{bmatrix}, \quad (1)$$

where f is the effective focal length; r is the aspect ratio; $\mathbf{p} = [u_0, v_0, 1]^T$ is the principal point and s the parameter describing the skew of the two image axes. Then the catadioptric image of a 3D space point \mathbf{X} is

$$\mathbf{m} = \lambda \mathbf{K} [\mathbf{I}, \xi \mathbf{e}] \begin{bmatrix} \mathbf{X} / \|\mathbf{X}\| \\ 1 \end{bmatrix} = \lambda \mathbf{K} (\mathbf{X} / \|\mathbf{X}\| + \xi \mathbf{e}), \quad (2)$$

where λ is a scalar, \mathbf{I} is an identical matrix, $\mathbf{e} = [0, 0, 1]^T$, and $\xi \mathbf{e}$ is the coordinate of the sphere center, which denotes the translation from viewing sphere coordinate system $\mathbf{O}-xyz$ to the pinhole coordinate system $\mathbf{O}^c-x^c y^c z^c$. In this imaging system, $[f, r, s, u_0, v_0, \xi]$ is the camera intrinsic parameter.

3. Constraints on camera parameters

In (Wu et al., 2008), the authors have derived the projection of a 3D space point as follows:

Proposition 1. Let \mathbf{m} be the catadioptric image of a space point \mathbf{X} . Then under the pinhole coordinate system $\mathbf{O}^c-x^c y^c z^c$, the projection of point \mathbf{X} on the viewing sphere can be expressed as:

$$\mathbf{X}^s = \frac{\xi(1 + \sqrt{1 + \tau\eta})}{\eta} \mathbf{K}^{-1} \mathbf{m}. \quad (3)$$

In the case of paraboloid mirror, i.e. $\xi = 1$,

$$\mathbf{X}^s = \frac{2}{\eta} \mathbf{K}^{-1} \mathbf{m}, \quad (4)$$

where $\tau = (1 - \xi^2) / \xi^2$, $\boldsymbol{\omega} = \mathbf{K}^{-T} \mathbf{K}^{-1}$ is the image of absolute conic (IAC) of the virtual pinhole camera, and $\eta = \mathbf{m}^T \boldsymbol{\omega} \mathbf{m}$ is the algebraic distance from the image point to IAC.

Based on Proposition 1, we have the following constraint on all the catadioptric parameters:

Proposition 2.. Let $\{\mathbf{m}_j : j = 1, 2, 3\}$ be the catadioptric image of three collinear space points $\{\mathbf{X}_j : j = 1, 2, 3\}$. Then,

$$\phi(\tau, \boldsymbol{\omega}) \triangleq \det \left[\begin{array}{c} \left((1 + \sqrt{1 + \tau\eta_1}) \mathbf{m}_1 - \eta_1 \mathbf{p}, (1 + \sqrt{1 + \tau\eta_2}) \mathbf{m}_2 - \eta_2 \mathbf{p}, \right. \\ \left. (1 + \sqrt{1 + \tau\eta_3}) \mathbf{m}_3 - \eta_3 \mathbf{p} \right) \end{array} \right] = 0, \quad (5)$$

where \det denotes determinant of a matrix, $\eta_j = \mathbf{m}_j^T \boldsymbol{\omega} \mathbf{m}_j$, $j = 1, 2, 3$, $\boldsymbol{\omega} = \mathbf{K}^{-T} \mathbf{K}^{-1}$

$$= \frac{1}{r^2 f^4} \begin{pmatrix} f^2 & -sf & sv_0 f - u_0 f^2 \\ -sf & s^2 + r^2 f^2 & su_0 f - s^2 v_0 - v_0 r^2 f^2 \\ sv_0 f - u_0 f^2 & su_0 f - s^2 v_0 - v_0 r^2 f^2 & (sv_0 - u_0 f)^2 + r^2 v_0^2 f^2 + r^2 f^4 \end{pmatrix}.$$

Proof. According to the unified sphere model, the projections of three collinear space points on the viewing sphere, $\{\mathbf{X}_j^s : j = 1, 2, 3\}$, should be on a great circle of the sphere. That is, the three unit vectors $\mathbf{O}\mathbf{X}_1^s, \mathbf{O}\mathbf{X}_2^s, \mathbf{O}\mathbf{X}_3^s$ are coplanar. Thus we have

$$\det [\mathbf{X}_1^s - \mathbf{O}, \mathbf{X}_2^s - \mathbf{O}, \mathbf{X}_3^s - \mathbf{O}] = 0. \quad (6)$$

By Eq. (3), we have

$$\begin{aligned} \mathbf{X}_j^s - \mathbf{O} &= \frac{\xi(1 + \sqrt{1 + \tau\eta_j})}{\eta_j} \mathbf{K}^{-1} \mathbf{m}_j - \xi \mathbf{e} \\ &= \xi \mathbf{K}^{-1} \left(\frac{(1 + \sqrt{1 + \tau\eta_j})}{\eta_j} \mathbf{m}_j - \mathbf{K} \mathbf{e} \right) \\ &= \frac{\xi \mathbf{K}^{-1}}{\eta_j} \left((1 + \sqrt{1 + \tau\eta_j}) \mathbf{m}_j - \eta_j \mathbf{p} \right). \end{aligned} \quad (7)$$

Since $\det \mathbf{K}^{-1} \neq 0$, we obtain

$$\begin{aligned} \det [\mathbf{X}_1^s - \mathbf{O}, \mathbf{X}_2^s - \mathbf{O}, \mathbf{X}_3^s - \mathbf{O}] &= \frac{\xi^3 \det \mathbf{K}^{-1}}{\eta_1 \eta_2 \eta_3} \det \left[\begin{array}{c} \left((1 + \sqrt{1 + \tau\eta_1}) \mathbf{m}_1 - \eta_1 \mathbf{p}, \right. \\ \left. (1 + \sqrt{1 + \tau\eta_2}) \mathbf{m}_2 - \eta_2 \mathbf{p}, \right. \\ \left. (1 + \sqrt{1 + \tau\eta_3}) \mathbf{m}_3 - \eta_3 \mathbf{p} \right) \end{array} \right] = 0 \\ &\propto \det \left[\begin{array}{c} \left((1 + \sqrt{1 + \tau\eta_1}) \mathbf{m}_1 - \eta_1 \mathbf{p}, \right. \\ \left. (1 + \sqrt{1 + \tau\eta_2}) \mathbf{m}_2 - \eta_2 \mathbf{p}, \right. \\ \left. (1 + \sqrt{1 + \tau\eta_3}) \mathbf{m}_3 - \eta_3 \mathbf{p} \right) \end{array} \right] = 0. \end{aligned} \quad (8)$$

Hence, the constraint holds. \square

Let

$$\mathbf{T}_p = \begin{bmatrix} 1 & 0 & -u_0 \\ 0 & 1 & -v_0 \\ 0 & 0 & 1 \end{bmatrix}, \quad \hat{\mathbf{K}} = \mathbf{T}_p \mathbf{K} = \begin{bmatrix} rf & s & 0 \\ 0 & f & 0 \\ 0 & 0 & 1 \end{bmatrix},$$

then $\hat{\mathbf{m}} = \mathbf{T}_p \mathbf{m}$ is a transformation translating the origin of the image plane to principal point \mathbf{p} . From Eq. (5), we have

$$\begin{aligned} \det(\mathbf{T}_p) \det \left[\begin{array}{c} \left((1 + \sqrt{1 + \tau\eta_1}) \mathbf{m}_1 - \eta_1 \mathbf{p}, (1 + \sqrt{1 + \tau\eta_2}) \mathbf{m}_2 \right. \\ \left. - \eta_2 \mathbf{p}, (1 + \sqrt{1 + \tau\eta_3}) \mathbf{m}_3 - \eta_3 \mathbf{p} \right) \end{array} \right] \\ = \det \left(\mathbf{T}_p \left[\begin{array}{c} (1 + \sqrt{1 + \tau\eta_1}) \mathbf{m}_1 - \eta_1 \mathbf{p}, (1 + \sqrt{1 + \tau\eta_2}) \mathbf{m}_2 \\ - \eta_2 \mathbf{p}, (1 + \sqrt{1 + \tau\eta_3}) \mathbf{m}_3 - \eta_3 \mathbf{p} \end{array} \right] \right) \\ = \det \left[\begin{array}{c} \left((1 + \sqrt{1 + \tau\eta_1}) \hat{\mathbf{m}}_1 - \eta_1 \mathbf{e}, (1 + \sqrt{1 + \tau\eta_2}) \hat{\mathbf{m}}_2 \right. \\ \left. - \eta_2 \mathbf{e}, (1 + \sqrt{1 + \tau\eta_3}) \hat{\mathbf{m}}_3 - \eta_3 \mathbf{e} \right) \end{array} \right] = 0. \end{aligned} \quad (9)$$

Let $\hat{\mathbf{m}}_i = (x_i, y_i, 1)^T$, then

$$\begin{aligned} \eta_i &= \mathbf{m}_i^T \boldsymbol{\omega} \mathbf{m}_i = \hat{\mathbf{m}}_i^T \mathbf{T}_p^{-T} \boldsymbol{\omega} \mathbf{T}_p^{-1} \hat{\mathbf{m}}_i \\ &= \frac{r^2 f^4 + (x_i^2 + y_i^2 r^2) f^2 - 2s x_i y_i f + y_i^2 s^2}{r^2 f^4}. \end{aligned}$$

Let

$$\begin{aligned} D_1 &= \det \begin{bmatrix} x_1 & x_2 \\ y_1 & y_2 \end{bmatrix}, \\ D_2 &= \det \begin{bmatrix} x_1 & x_3 \\ y_1 & y_3 \end{bmatrix}, \\ D_3 &= \det \begin{bmatrix} x_2 & x_3 \\ y_2 & y_3 \end{bmatrix}. \end{aligned} \quad (10)$$

When $\tau = 0$, i.e. in the case of para-catadioptric camera, from Eq. (9), we have:

$$\begin{aligned} \det[2\hat{\mathbf{m}}_1 - \eta_1 \mathbf{e}, 2\hat{\mathbf{m}}_2 - \eta_2 \mathbf{e}, 2\hat{\mathbf{m}}_3 - \eta_3 \mathbf{e}] &= D_3 \eta_1 - D_2 \eta_2 + D_1 \eta_3 \\ &- 2(D_3 - D_2 + D_1) = 0 \\ &\propto (D_3 - D_2 + D_1) r^2 f^4 - (D_3 x_1^2 - D_2 x_2^2 + D_1 x_3^2) f^2 \\ &- (D_3 y_1^2 - D_2 y_2^2 + D_1 y_3^2) r^2 f^2 + 2(D_3 x_1 y_1 - D_2 x_2 y_2 + D_1 x_3 y_3) s f \\ &- (D_3 y_1^2 - D_2 y_2^2 + D_1 y_3^2) s^2 = 0. \end{aligned} \quad (11)$$

When all other parameters are known, Eq. (11) gives a polynomial constraint with degree 4 on the effective focal length, and a linear constraint on the effective focal length square if $s = 0$ or $s = \delta f$ with δ being a constant. So, given the image points of any three collinear space points, the effective focal length can be determined directly by solving the Eq. (11).

Let $\hat{\boldsymbol{\omega}} = \mathbf{T}_p^{-T} \boldsymbol{\omega} \mathbf{T}_p^{-1} = \hat{\mathbf{K}}^{-T} \hat{\mathbf{K}}^{-1} = \begin{pmatrix} \hat{\omega}_{11} & \hat{\omega}_{21} & 0 \\ \hat{\omega}_{12} & \hat{\omega}_{22} & 0 \\ 0 & 0 & 1 \end{pmatrix}$, $\hat{\omega}_{12} = \hat{\omega}_{21}$. From Eq. (11), we get

$$\begin{aligned} (D_3 x_1^2 - D_2 x_2^2 + D_1 x_3^2) \hat{\omega}_{11} + (D_3 y_1^2 - D_2 y_2^2 + D_1 y_3^2) \hat{\omega}_{22} \\ + 2(D_3 x_1 y_1 - D_2 x_2 y_2 + D_1 x_3 y_3) \hat{\omega}_{21} = D_3 - D_2 + D_1 \end{aligned} \quad (12)$$

Apparently, Eq. (12) is a linear constraint on the unknown items of the matrix $\hat{\boldsymbol{\omega}}$. So, given three triples of image points of collinear space points, with the principal point known, we can linearly estimate the matrix $\hat{\boldsymbol{\omega}}$. Then the effective focal length, the aspect ratio and the skew can be obtained by matrix decomposition for the matrix $\hat{\boldsymbol{\omega}}$. In fact, the constraint in Eq. (12) is equivalent to the constraint used in (Wu et al., 2006). The difference is that the constraint here is deduced from the projections of three collinear space points on the viewing sphere, while the one in (Wu et al., 2006) is from a rectified perspective image.

When $\tau \neq 0$, i.e. in the case of ellipsoid or hyperboloid mirror, by Eq. (9), we have:

$$\begin{aligned} \det \left[\begin{array}{c} \left((1 + \sqrt{1 + \tau\eta_1}) \hat{\mathbf{m}}_1 - \eta_1 \mathbf{e}, (1 + \sqrt{1 + \tau\eta_2}) \hat{\mathbf{m}}_2 - \eta_2 \mathbf{e}, \right. \\ \left. (1 + \sqrt{1 + \tau\eta_3}) \hat{\mathbf{m}}_3 - \eta_3 \mathbf{e} \right) \end{array} \right] = 0 \\ \propto \det \left[\begin{array}{c} \hat{\mathbf{m}}_1 + \frac{1 - \sqrt{1 + \tau\eta_1}}{\tau} \mathbf{e}, \hat{\mathbf{m}}_2 - \frac{1 - \sqrt{1 + \tau\eta_2}}{\tau} \mathbf{e}, \\ \hat{\mathbf{m}}_3 - \frac{1 - \sqrt{1 + \tau\eta_3}}{\tau} \mathbf{e} \end{array} \right] = 0 \\ \propto \det \begin{bmatrix} x_1 & x_2 & x_3 \\ y_1 & y_2 & y_3 \\ (1 + \tau) r f^2 - \sqrt{\lambda_1} & (1 + \tau) r f^2 - \sqrt{\lambda_2} & (1 + \tau) r f^2 - \sqrt{\lambda_3} \end{bmatrix} = 0 \\ \propto D_3 \sqrt{\lambda_1} - D_2 \sqrt{\lambda_2} + D_1 \sqrt{\lambda_3} - (1 + \tau)(D_3 - D_2 + D_1) r f^2 = 0 \end{aligned} \quad (13)$$

where $\lambda_i = (1 + \tau) r^2 f^4 + \tau(x_i^2 + y_i^2 r^2) f^2 - 2\tau s x_i y_i f + \tau y_i^2 s^2$. It will become a polynomial constraint with degree 16 on the effective focal length by removing the radical sign, which can be realized by using the symbolic computation function of the software MAPLE. If $s = 0$ or $s = \delta f$ with δ being a constant, it will become a polynomial constraint with degree 4 on the effective focal length square. See concrete forms in Appendix A.

4. Calibrating algorithm

Generally, there are totally six parameters $[f, r, s, u_0, v_0, \xi]$ to be determined in central catadioptric camera calibration. However, the focal length is the most important parameter to be estimated, while other parameters can be obtained by prior information about scene or system configuration. For example, due to highly advanced manufacturing technology, the principal point can be set as the image center or determined from the bounding ellipse of the catadioptric image (Kang, 2000), the skew can be considered as zero, the aspect ratio as one and the mirror parameter can be computed from the eccentricity of the mirror. Here we only estimate the effective focal length with the assumption that all the other parameters are known.

Previous approaches using lines have to fit conics to line images. However, it is very difficult to get the conics correctly even for a lower noise level due to partial occlusions. Thus the constraints derived from the conics are largely biased. Instead we use the constraint of Eq. (11) or Eq. (13) from three image points on a line image. For estimation of the effective focal length f , a triple of image points on one line image is enough, and more triples can improve the calculation stability.

4.1. Algorithm implementation

Given the catadioptric image of a space line, and denote the detected image point set of the space line as \mathbf{D} . Assume all other parameters are known, the estimation algorithm for the effective focal length is as follows:

- Step 1. On the line image, randomly choose M ($M \geq 1$) triples of image points, and establish a constraint Eqs. (11), (13) using each triple of image points.
- Step 2. Get one estimate of the effective focal length from each constraint equation, and totally M estimates are obtained.
- Step 3. Sort the M estimates, and discard k ($0 \leq k < M/2$) inferior estimates on the head and tail respectively.
- Step 4. For each of the reserved estimates, compute a projection set \mathbf{Q} of the image point set \mathbf{D} on the viewing sphere using Eq. (3), and determine a plane through the viewing sphere center \mathbf{O} and the projection set \mathbf{Q} .
- Step 5. Compute a distance sum from the points of each projection set \mathbf{Q} to its corresponding plane determined in Step 4, and choose the estimate corresponding to the least distance sum as the final output.

Remark 1. For improving calculation stability, the selected three image points in Step 1 should be scattered on the line image. Here we use distance measure to reject the bad sampling. In Step 2, according to the fundamental theorem of algebra, one polynomial constraint equation with degree d has d complex roots. However, only one root is valid since the effective focal length is unique for a specific image. We find in experiments that other real roots are very close to zero or negative.

Remark 2. This algorithm is similar to RANSAC (Fischler and Bolles, 1981), so the sampling number M can be decided by the technique in RANSAC. Since the sampling is in a random way, the estimate of the effective focal length should be in a normal distribution with the mean value being optimal. Step 3 is optional, and discarding $2k$ estimates is to accelerate this algorithm. The accuracy of the algorithm will hardly be affected when excluding Step 3. In our implementation, M is 50, and k is 20.

Remark 3. In Step 5, assume that the unit normal vector of the plane is \mathbf{n} and the projection set

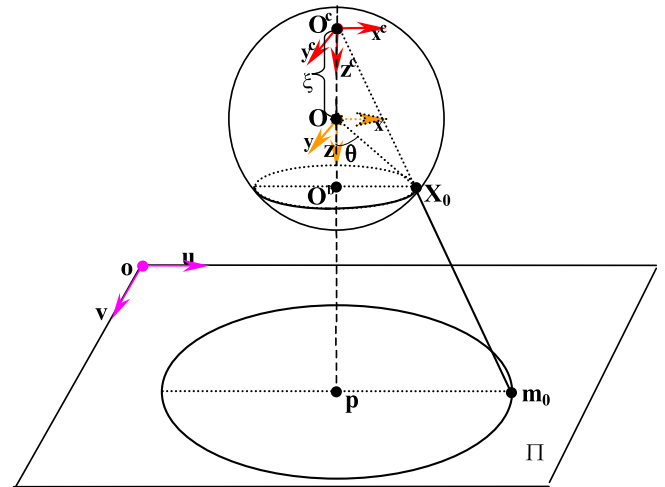


Fig. 2. The mirror boundary and its image.

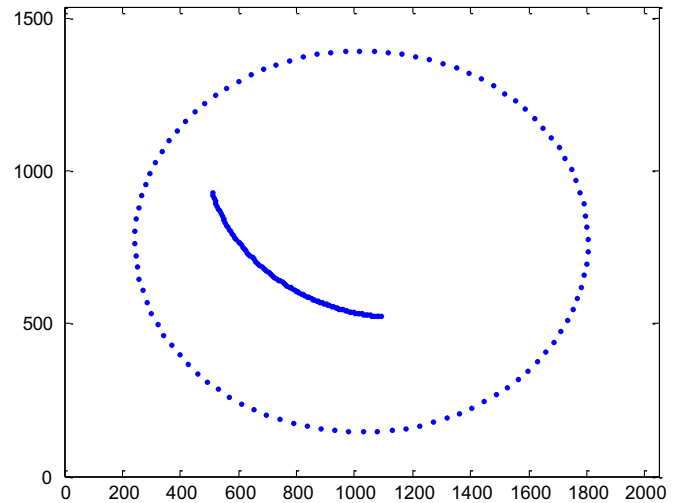


Fig. 3. Bounding ellipse and the used line image.

$$\mathbf{Q} = \{\mathbf{X}_i^s, i = 1, 2, \dots, m\}.$$

We can build the following vector equation:

$$\mathbf{A}\mathbf{n} = \mathbf{0} \quad \text{with} \quad \|\mathbf{n}\| = 1, \quad (14)$$

where $\mathbf{A} = [\mathbf{X}_1^s - \mathbf{O}, \mathbf{X}_2^s - \mathbf{O}, \dots, \mathbf{X}_m^s - \mathbf{O}]^T$. The normal vector \mathbf{n} can be solved in the least square sense by using SVD method, and the distance sum from the projection set to the plane in Step 5 is equal to the minimal singular value.

4.2. Calibration using multiple lines

In real applications, we can detect more than one line image because usually there are many space lines in real scenes. Since each line image has different partial occlusion and noise level, the result estimated from each line is different. In order to improve the estimation accuracy, we suggest calibration using multiple lines, where the above algorithm is performed respectively for each line image. However, there is a minor revision on the algorithm in each trail as follows: Firstly, in Step 4, the projections on the viewing sphere are computed not for a single space line but for all space lines, and not a plane but all the planes corresponding to each

space line are determined from the viewing sphere center O and their corresponding projections; Secondly, in Step 5, the distance sum is computed from the projections, which belong to not a single but all the space lines, to their corresponding plane.

4.3. Other parameters determination

In fact, since the eccentricity of the mirror is usually known, and is very accurate, the mirror parameter ξ can be obtained from the eccentricity ε of the mirror as (Geyer and Daniilidis, 2001):

$$\xi = \frac{2\varepsilon}{1 + \varepsilon^2}, \tag{15}$$

Here, we mainly discuss the determination of other four parameters $[r, s, u_0, v_0]$ from the bounding ellipse of the catadioptric image.

In central catadioptric cameras, the mirror boundary is a circle, and is projected to an ellipse by the traditional camera, which is called the bounding ellipse. Ideally, the optical axis of the traditional camera is perpendicular to the plane containing the circle and goes through the center of the circle, so center of the bounding ellipse is the principal point. Generally, unlike the catadioptric image of a space line, the bounding ellipse is a whole big conic (see Figs. 4a and 5a), so it can be fitted well using existing techniques (Fitzgibbon et al., 1999). In (Ying and Hu, 2004; Kang, 2000), partial intrinsic parameters of the camera can be determined from the bounding ellipse of the catadioptric image. Assume the bounding ellipse is estimated as

$$ax^2 + 2bxy + cy^2 + 2dx + 2ey + h = 0. \tag{16}$$

The authors of Ying and Hu (2004) give the following estimation:

$$\begin{cases} r = \sqrt{-\frac{b^2}{a^2} + \frac{c}{a}} \\ \frac{s}{f} = -\frac{b}{a} \\ u_0 = \frac{be - cd}{ac - b^2} \\ v_0 = \frac{bd - ae}{ac - b^2} \end{cases} \tag{17}$$

In the following, we analyze the sensitivity of the estimation to system configuration and image noises. In the generalized imaging model (see Fig. 2), the optical axes of the virtual pinhole camera is the line going through the viewpoints O and O^c , the mirror boundary of the catadioptric camera corresponds to a little circle vertical to the line OO^c , which is decided by field of view (FOV) of the central catadioptric camera, and there is only a translation between the pinhole coordinate system $O^c-x^c y^c z^c$ and sphere coordinate system $O-xyz$. In real configurations, the optical axes maybe

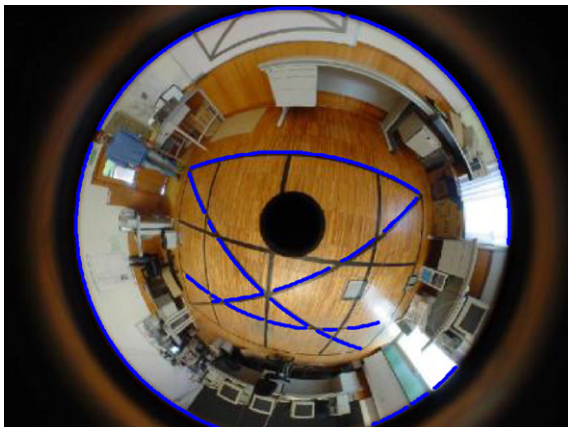


Fig. 4a. The used lines and the mirror boundary with paracatadioptric camera.

slightly deviate from the line OO^c , that is, a small rotation between the two coordinate systems exists. Let the rotation be R , then the catadioptric image of a 3D space point X becomes

$$m = \lambda K[R, \xi e] \begin{bmatrix} X/\|X\| \\ 1 \end{bmatrix}. \tag{18}$$

Next we analyze the effect of the rotation R by simulation.

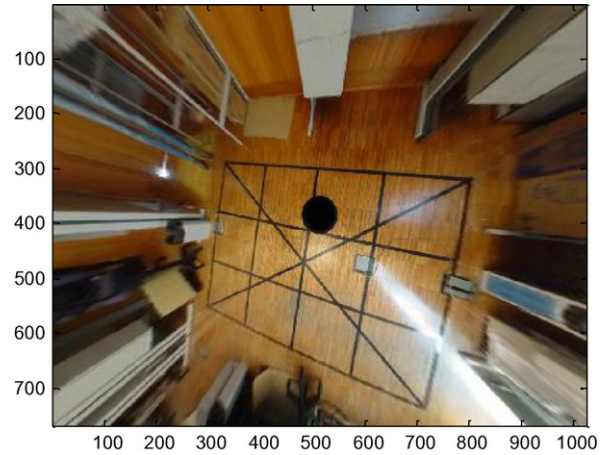


Fig. 4b. The rectified paracatadioptric image by the proposed algorithm.

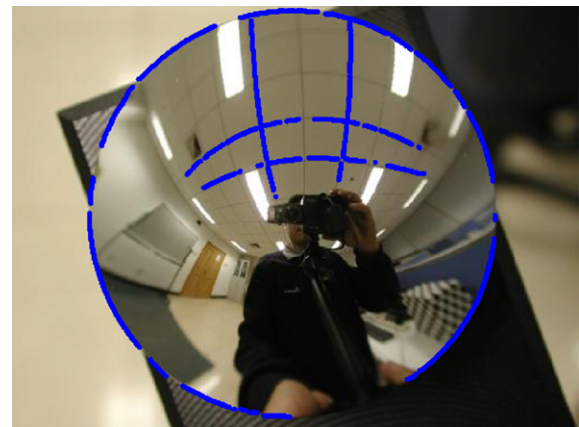


Fig. 5a. The used lines and the mirror boundary with hypercatadioptric camera.

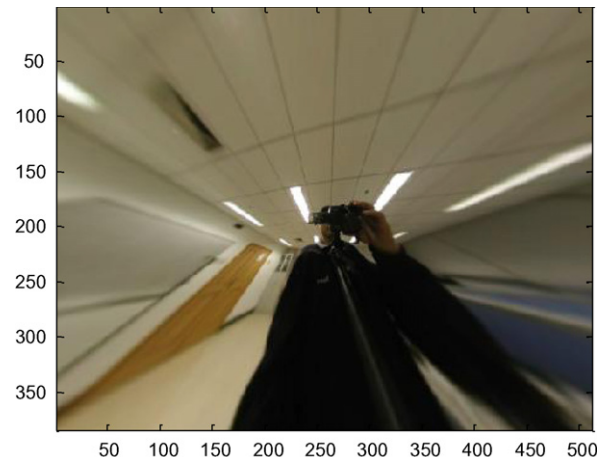


Fig. 5b. The rectified hypercatadioptric image by the proposed algorithm.

The parameters of the simulated catadioptric camera are $(rf, f, s, u_0, v_0, \xi) = (260, 240, 1, 512, 384, 0.96)$, and FOV is 210-degree. The rotations are generated by rotating the line \mathbf{OO}^c around the viewpoint \mathbf{O}^c with an angle, which is 0, 0.3, 0.6, 0.9 degree respectively. The mirror boundary is projected by Eq. (18). For each rotation angle, we perform 100 independent trails. In each trail, Gaussian noise with zero mean and standard deviation $\sigma = 5$ pixels is added to each image point of the mirror boundary. Means and standard deviations of the estimated parameters in Eq. (17) are shown in Table 1. We can see from the table that the principal point and the aspect ratio r are not sensitive to image noise, the aspect ratio r is hardly influenced by the rotation angle, and the principal point is very close to real value with standard deviation increasing gradually by the variation of the rotation angle. We also can see the ratio s/f is not reliable due to image noise and the rotation. However, the skew s is very little in real case, and nearly can be neglected, so the ratio s/f will have a little impact on effective focal length estimation.

5. Experimental results

In this section, we use simulated and real data to evaluate the performance of the proposed algorithm. The boundary ellipse is fitted using the algorithm in (Fitzgibbon et al., 1999).

5.1. Simulations

The intrinsic parameters of the simulated catadioptric cameras are $(rf, f, s, u_0, v_0, \xi) = (500, 400, 1, 1024, 768, 0.9)$, and the FOV is 210-degree. One catadioptric line image is randomly generated by choosing one unit normal vector corresponding to a great circle on the viewing sphere. To simulate actual conditions, we choose 100 points on a one-third portion of the entire circle, and project these points to the catadioptric image plane. The generated line image is shown in Fig. 3. Gaussian noise with zero mean and standard deviation σ is added to each image point of the space line and the principal point as well. The noise level σ is varied from 0 to 5 pixels with a step of one pixel. For each noise level, we perform 100 trails. In each trail, the aspect ratio r and the ratio s/f is set by adding Gaussian noise with zero mean and standard deviation $\sigma_1 = 0.005$ to their real values respectively. Means and standard deviations of the estimated effective focal length with respect to different noise levels are shown in Table 2. From the table, we can see that the mean values are very close to the ground truth in every noise level, and the standard deviation is increased gradually with the raising of the noise level. We also perform the sim-

Table 1 Means and standard deviations of the estimated parameters from the mirror boundary.

Rotation Angle	u_0	v_0	r	s/f
	512	384	1.0833	0.0042
0	512.0 ± 0.66	384.0 ± 0.66	1.0830 ± 0.0041	0.0037 ± 0.0039
0.3	512.0 ± 1.69	383.9 ± 1.52	1.0838 ± 0.0043	0.0041 ± 0.0041
0.6	512.0 ± 2.98	383.6 ± 2.62	1.0838 ± 0.0049	0.0039 ± 0.0041
0.9	512.8 ± 3.97	384.9 ± 4.12	1.0835 ± 0.0046	0.0040 ± 0.0044

Table 2 Means and standard deviations of the estimated effective focal length.

Noise	0	1	2	3	4	5
Mean	399.82	400.09	400.37	400.94	400.67	401.48
Standard deviation	2.06	2.80	3.60	4.30	5.78	6.00

ulation for $\xi = 1$, i.e. for para-catadioptric camera, the result is similar. It shows that the proposed method is effective and robust. In essence, the algorithm is similar to RANSAC, and a good estimation can be obtained as long as one good sampling exists among all samplings.

5.2. Real data

5.2.1. With paracatadioptric camera

Fig. 4a shows an image with a resolution of 1024×768 downloaded from <http://mail.isr.uc.pt/~carloss/software/software.htm>, which is acquired by an uncalibrated paracatadioptric camera. Its field of view (FOV) is 180° Barreto and Araujo, 2006. Four line images are selected and shown in the figure. The used points on the line images and the boundary ellipse are manually selected using the software presented in this website. The camera parameters estimated from the bounding ellipse of the catadioptric image are $(r, s/f, u_0, v_0) = (0.9993, 3.94e - 4, 520.3, 395.7)$. As described in Section 4, to improve estimation accuracy, we use the four line images. The estimated effective focal length is 318.73. In order to validate the estimation, we rectify the original distorted image using the estimated parameters. Since the camera’s FOV is large, we only show some part of the rectified image in Fig. 4b. We can clearly see the rectified lines are very straight. The estimation result by the algorithm in (Wu et al., 2006) (hereafter called DLP) is $(r, s, f) = (1.01, 4.3, 313.15)$, which is estimated with the condition that the principal point is known. We also perform the algorithms proposed in (Barreto and Araujo, 2005 and (Wu et al., 2008), which need fit conics to line images, hereafter called CP and CLP respectively. Since the approach in (Barreto and Araujo, 2006 for conic fitting of line images in paracatadioptric systems is effective, it is used here in performing CP and CLP. When fitting conics to the line images, we use the prior information that the aspect ratio is 1. Estimation results of the camera parameters using these conics of the line images are $(rf, f, s, u_0, v_0, \xi) = (319.3, 3, 9.3, -0.0225, 516.9, 394.1, 1)$ and $(rf, f, s, u_0, v_0, \xi) = (318.95, 31, 8.66, 0.0092, 516.9, 394.1, 1)$ by CP and CLP respectively. We can see that all the estimation results are very close to the one using the proposed method. For a quantitative comparison, we transform the catadioptric image into a perspective image by using these estimation results of the camera parameters respectively, and compute the fitting error of the four lines in the perspective image. Since both the proposed method and DLP need random sampling of image points, we perform 200 times of calibrations by the proposed method and DLP respectively, and compute the mean and standard deviation of the fitting error. The fitting errors of the four algorithms are shown in Table 3. From the table, we can see that the mean values are close to each other; while the standard deviation of DLP is larger than the one of the proposed method. It shows that the proposed method is more stable than DLP. In principle, the proposed method is a robust estimation technique, and the final estimation result is determined by the best one among all samplings, whereas the estimation result of DLP is determined by all samplings, which probably include some bad ones. Both methods need some parameters known in advance, so they will be influenced by the known parameters to some extent. In CP and CLP, conic fitting of the line images is indispensable, and the estimation result is susceptible to quality of the conic

Table 3 The fitting error of the four algorithms.

Algorithm	The proposed	DLP	CP	CLP
Mean	0.3815	0.3829	0.3929	0.4032
Standard deviation	0.0018	0.0103	–	–

fitting. A significant estimation can be obtained with an effective conic fitting of the line images since the two algorithms estimate all parameters by the constraints from the fitted conics. However, the approach in (Barreto and Araujo, 2006) for conic fitting of line images only work for paracatadioptric images, and there is still not an effective way for other types of catadioptric images. In the following, we will show another case with hypercatadioptric camera.

5.2.2. With hypercatadioptric camera

The used catadioptric system consists of a NIKON COOLPIX990 camera and a hyperbolic mirror. The mirror is designed by the Center for Machine Perception, Czech Technical University, its FOV is 217.2° , and the eccentricity of the hyperbolic mirror is 1.302, corresponding to $\xi = 0.966$. One image of an indoor scene is taken with a resolution of 512×384 . Four lines are used and shown in Fig. 5a. The intrinsic parameters of the camera estimated from the bounding ellipse of the catadioptric image are $(r, s/f, u_0, v_0) = (0.9994, -5.83e - 5, 254.4, 188.5)$. The estimated effective focal length using the four line images is 141.6. The rectified image by this estimation result is shown in Fig. 5b. On the contrary, calibrations by CP and CLP are not solvable due to bad conic fitting of the line images. Similar to the paracatadioptric case, the estimation by DLP is less stable than the one by the proposed method.

5.2.3. With calibration object

We use the same hypercatadioptric camera to take pictures of a calibration object from four different viewpoints, one of which is shown in Fig. 6. 25 image points of five space lines of a plane is chosen manually as Fig. 6 shows. The paper (Kannala et al., 2008) gives an extensive discussion on camera calibration using a calibration object. Here we calibrate the images by the proposed method and the approach in (Kannala et al., 2008) respectively. When performing the calibration in (Kannala et al., 2008), we use the calibration toolbox that the author provides, where different imaging models are used. RMS of the reprojection error of the 25 space points is computed for different models and different methods, which is shown in Table 4. Details on the imaging models can be seen in (Kannala et al., 2008). From the table, we can see that the reprojection error of the proposed method is less than the one of the M6 model and larger than the ones of the other two models. The models in (Kannala et al., 2008) include distortion terms that model the possible imperfections in the optical system. The M23 and M9 have more distortion terms than M6, so maybe the two models are more accurate. On the other side, the calibration in (Kannala et al. 2008) is based on 2D–3D point correspondences, which usually is thought of high accuracy, while the proposed method does not use the accurate 3D space information. Compar-



Fig. 6. Image of a calibration object.

Table 4
RMS of the reprojection error.

Method	The proposed method	M6	M9	M23
RMS of reprojective error	2.001	3.350	1.770	1.031

atively, the proposed method is more flexible and suitable for automated calibration.

6. Conclusion

Nearly all central catadioptric calibration approaches using lines need conic fitting of line images, which is hard to accomplish and highly affects the calibration accuracy. In this paper, we present a polynomial constraint on the effective focal length of central catadioptric cameras, which is based on a property that the projections of any three collinear space points on the viewing sphere should be coplanar with the view sphere center. Based on this constraint, we propose a simple method for estimation of the effective focal length of central catadioptric cameras. The method needs no conic fitting of line images, and is easy to implement. Only a single view of one space line is enough to estimate the effective focal length, and no other space information is needed. Experiments on simulated and real data show the proposed method is robust and effective.

Acknowledgments

This work was partially supported by the National Natural Science Foundation of China (Nos. 60872127, 60736008, 61005039), National High-Tech Research and Development 863 Plan of China (No. 2008AA01Z301), the open projects program of National Laboratory of Pattern Recognition of Institute of Automation, Chinese Academy of Sciences under Grant No. 20090096.

Appendix A

Denote Eq. (13) as,

$$a1\sqrt{\lambda_1} + a2\sqrt{\lambda_2} + a3\sqrt{\lambda_3} + a4f^2 = 0, \quad (19)$$

where,

$$\lambda_1 = b1f^4 + c1f^2 + d1f + e1,$$

$$\lambda_2 = b2f^4 + c2f^2 + d2f + e2,$$

$$\lambda_3 = b3f^4 + c3f^2 + d3f + e3.$$

Then, by removing radical sign with the software MAPLE, Eq. (19) becomes a polynomial equation with degree 16 on the effective focal length f as follows:

$$\begin{aligned} &16a3^2a4^2f^4(a2^2(b2f^4 + c2f^2 + d2f + e2) - a4^2f^4 + a1^2(b1f^4 \\ &+ c1f^2 + d1f + e1) - a3^2(b3f^4 + c3f^2 + d3f + e3))^2(b3f^4 + c3f^2 \\ &+ d3f + e3) - (-2a2^2(b2f^4 + c2f^2 + d2f + e2)a3^2(b3f^4 + c3f^2 \\ &+ d3f + e3) + a1^4(b1f^4 + c1f^2 + d1f + e1)^2 - 2a2^2(b2f^4 + c2f^2 \\ &+ d2f + e2)a4^2f^4 - 2a1^2(b1f^4 + c1f^2 + d1f + e1)a2^2(b2f^4 + c2f^2 \\ &+ d2f + e2) - 2a1^2(b1f^4 + c1f^2 + d1f + e1) + a3^2(b3f^4 + c3f^2 \\ &+ d3f + e3) + a4^4f^8 + a2^4(b2f^4 + c2f^2 + d2f + e2)^2 + a3^4(b3f^4 \\ &+ c3f^2 + d3f + e3)^2 - 2a1^2(b1f^4 + c1f^2 + d1f + e1)a4^2f^4 \\ &+ 6a3^2(b3f^4 + c3f^2 + d3f + e3)a4^2f^4)^2 = 0. \quad (20) \end{aligned}$$

Since the canonical form of Eq. (20) is too long, we do not show it here.

If $s = 0$ or $s = \delta f$ with δ being a constant, Eq. (19) becomes a polynomial equation with degree 4 on the effective focal length square as follows:

$$F18f^8 + F17f^6 + F16f^4 + F15f^2 + F14 = 0, \quad (21)$$

where,

$$F14 = -(-2a^2(c2 + d2 + e2)a^3(c3 + d3 + e3) + a^3^4(c3 + d3 + e3)^2 + a^2^4(c2 + d2 + e2)^2 + a^1^4(c1 + d1 + e1)^2 - 2a^1^2(c1 + d1 + e1)a^2^2(c2 + d2 + e2) - 2a^1^2(c1 + d1 + e1)a^3^2(c3 + d3 + e3))^2,$$

$$F15 = 16a^3^2a^4^2(a^2^2(c2 + d2 + e2) - a^3^2(c3 + d3 + e3) + a^1^2(c1 + d1 + e1))^2(c3 + d3 + e3) - 2(-2a^2^2(c2 + d2 + e2)a^3^2(c3 + d3 + e3) + a^3^4(c3 + d3 + e3)^2 + a^2^4(c2 + d2 + e2)^2 + a^1^4(c1 + d1 + e1)^2 - 2a^1^2(c1 + d1 + e1)a^2^2(c2 + d2 + e2) - 2a^1^2(c1 + d1 + e1)a^3^2(c3 + d3 + e3))(-2a^2^2(c2 + d2 + e2)a^3^2b3 - 2a^2^2b2a^3^2(c3 + d3 + e3) - 2a^2^2(c2 + d2 + e2)a^4^2 + 2a^1^4(c1 + d1 + e1)b1 - 2a^1^2(c1 + d1 + e1)a^2^2b2 - 2a^1^2b1a^2^2(c2 + d2 + e2) + 6a^3^2(c3 + d3 + e3)a^4^2 + 2a^3^4(c3 + d3 + e3)b3 - 2a^1^2(c1 + d1 + e1)a^3^2b3 - 2a^1^2b1a^3^2(c3 + d3 + e3) - 2a^1^2(c1 + d1 + e1)a^4^2 + 2a^2^4(c2 + d2 + e2)b2),$$

$$F16 = 16a^3^2a^4^2(a^2^2(c2 + d2 + e2) - a^3^2(c3 + d3 + e3) + a^1^2(c1 + d1 + e1))^2b3 + 32a^3^2a^4^2(a^2^2(c2 + d2 + e2) - a^3^2(c3 + d3 + e3) + a^1^2(c1 + d1 + e1))(-a^4^2 + a^1^2b1 + a^2^2b2 - a^3^2b3)(c3 + d3 + e3) - 2(-2a^2^2(c2 + d2 + e2) \times a^3^2(c3 + d3 + e3) + a^3^4(c3 + d3 + e3)^2 + a^2^4(c2 + d2 + e2)^2 + a^1^4(c1 + d1 + e1)^2 - 2a^1^2(c1 + d1 + e1)a^2^2(c2 + d2 + e2) - 2a^1^2(c1 + d1 + e1)a^3^2(c3 + d3 + e3))(-2a^1^2b1a^3^2b3 + a^4^4 - 2a^2^2b2a^3^2b3 + a^3^4b3^2 - 2a^1^2b1a^2^2b2 + a^1^4b1^2 - 2a^1^2b1a^4^2 + a^2^4b2^2 - 2a^2^2b2a^4^2 + 6a^3^2b3a^4^2) - (-2a^2^2(c2 + d2 + e2)a^3^2b3 - 2a^2^2b2a^3^2(c3 + d3 + e3) - 2a^2^2(c2 + d2 + e2)a^4^2 + 2a^1^4(c1 + d1 + e1)b1 - 2a^1^2(c1 + d1 + e1)a^2^2b2 - 2a^1^2b1a^2^2(c2 + d2 + e2) + 6a^3^2(c3 + d3 + e3)a^4^2 + 2a^3^4(c3 + d3 + e3)b3 - 2a^1^2(c1 + d1 + e1)a^3^2b3 - 2a^1^2b1a^3^2(c3 + d3 + e3) - 2a^1^2(c1 + d1 + e1)a^4^2 + 2a^2^4(c2 + d2 + e2)b2)^2,$$

$$F17 = 32a^3^2a^4^2(a^2^2(c2 + d2 + e2) - a^3^2(c3 + d3 + e3) + a^1^2(c1 + d1 + e1))(-a^4^2 + a^1^2b1 + a^2^2b2 - a^3^2b3)b3 + 16a^3^2a^4^2(-a^4^2 + a^1^2b1 + a^2^2b2 - a^3^2b3)^2(c3 + d3 + e3) - 2(-2a^2^2(c2 + d2 + e2)a^3^3b3 - 2a^2^2b2a^3^2(c3 + d3 + e3) - 2a^2^2(c2 + d2 + e2)a^4^2 + 2a^1^4(c1 + d1 + e1)b1 - 2a^1^2(c1 + d1 + e1)a^2^2b2 - 2a^1^2b1a^2^2(c2 + d2 + e2) + 6a^3^2(c3 + d3 + e3)a^4^2 + 2a^3^4(c3 + d3 + e3)b3 - 2a^1^2(c1 + d1 + e1)a^3^2b3 - 2a^1^2b1a^3^2(c3 + d3 + e3) - 2a^1^2(c1 + d1 + e1)a^4^2 + 2a^2^4(c2 + d2 + e2)b2)(-2a^1^2b1a^3^2b3 + a^4^4 - 2a^2^2b2a^3^2b3 + a^3^4b3^2 - 2a^1^2b1a^2^2b2 + a^1^4b1^2 - 2a^1^2b1a^4^2 + a^2^4b2^2 - 2a^2^2b2a^4^2 + 6a^3^2b3a^4^2),$$

$$F18 = 16a^3^2a^4^2(-a^4^2 + a^1^2b1 + a^2^2b2 - a^3^2b3)^2b3 - (-2a^1^2b1a^3^2b3 + a^4^2 - 2a^2^2b2a^3^2b3 + a^3^4b3^2 - 2a^1^2b1a^2^2b2 + a^1^4b1^2 - 2a^1^2b1a^4^2 + a^2^4b2^2 - 2a^2^2b2a^4^2 + 6a^3^2b3a^4^2)^2.$$

References

Baker, S., Nayer, S., 1999. A theory of single-viewpoint catadioptric image formation. *IJCV* 35 (2), 175–196.
 Barreto, J.P., Araujo, H., 2005. Geometric properties of central catadioptric line images and their application in calibration. *IEEE Trans. PAMI* 27 (8), 1327–1333.
 Barreto, J.P., Araujo, H., 2006. Fitting conics to paracatadioptric projection of lines. *Computer Image and Vision Understanding* 101 (3), 151–165.
 Deng, X.M., Wu, F.C., Duan, F.Q., et al., 2007. Catadioptric camera calibration with one-dimensional objects. *Chinese J. Comput.* 30 (5), 737–747.
 Duan, F.Q., Wu, F.C., Hu, Z.Y., 2008. Pose determination and plane measurement using a trapezium. *Pattern Recognit. Lett.* 29 (3), 223–231.
 Fischler, M.A., Bolles, R.C., 1981. Random sample consensus: A paradigm for model fitting with applications to image analysis and automated cartography. *Commun. ACM* 24, 381–395.
 Fitzgibbon, A., Pilu, M., Fisher, R., 1999. Direct least square fitting of ellipses. *IEEE Trans. Pattern Anal. Mach. Intell.* 21 (5), 476–480.
 Geyer, C., Daniilidis, K., 1999. Catadioptric camera calibration. In: *Proceedings of 7th ICCV Vol. I* 398–404.
 Geyer, C., Daniilidis, K., 2001. Catadioptric projective geometry. *IJCV* 45 (3), 223–243.
 Geyer, C., Daniilidis, K., 2002. Paracatadioptric camera calibration. *IEEE Trans. Pattern Anal. Mach. Intell.* 24 (5), 687–695.
 Kang, S., 2000. Catadioptric self calibration. *CVPR Vol.1*, 201–207.
 Kannala, Juho, Heikkil, Janne, Brandt, SamiS., 2008. *Geometric camera calibration*. Wiley Encyclopedia of Computer Science and Engineering.
 Ramalingam, S., Sturm, P., Lodha, S.K., 2005. Towards generic self-calibration of central cameras, *The 6th Workshop on Omnidirectional Vision, Camera Networks and Non-classical Cameras*, in conjunction with ICCV 2005, pp. 20–27.
 Scaramuzza, D., Martinelli, A., Siegwart, R., 2006. A flexible technique for accurate omnidirectional camera calibration and structure from motion. In: *Proceedings of International Conference on Computer Vision Systems*. IEEE, 2006. 45–45.
 Sturm, P., Ramalingam, S., 2004. A generic concept for camera calibration. *ICCV*, 1–13.
 Sturm, P., Cheng, Z.L., Chen, P.C.Y., Poo, A.N., 2005. Focal length calibration from two views: Method and analysis of singular cases. *Computer Image and Vision Understanding* 99, 58–95.
 Swaminathan, R., Grossberg, M.D., Nayar, S., 2006. Non-single viewpoint catadioptric cameras: Geometry and analysis. *IJCV* 66 (3), 211–229.
 Wu, Y.H., Hu, Z.Y., 2005. Geometric invariants and applications under catadioptric camera model. *ICCV II*, 1547–1554.
 Wu, Y., Li, Y., Hu, Z., 2006. Easy calibration for para-catadioptric-like camera. In: *IEEE International Conference on Intelligent Robots and Systems*, 5719–5724.
 Wu, F.C., Duan, F.Q., Hu, Z.Y., et al., 2008. A new linear algorithm for calibrating central catadioptric cameras. *Pattern Recognit.* 41 (3), 3166–3172.
 Yagi, Y., Yachida, M., 2004. Real-time omnidirectional image sensors. *IJCV* 58 (3), 173–207.
 Ying, X.H., Hu, Z.Y., 2004. Catadioptric camera calibration using geometric invariants. *IEEE Trans. Pattern Anal. Mach. Intell.* 26 (10), 1260–1271.
 Ying, X.H., Zha, H.B., 2008. Identical projective geometric properties of central catadioptric line images and sphere images with applications to calibration. *IJCV* 78, 89–105.